Article:
Alonso, C, Ansola, R and Querin, OM (2014) Topology synthesis of multi-material compliant mechanisms with a Sequential Element Rejection and Admission method. Finite Elements in Analysis and Design, 85. 11 - 19. ISSN 0168-874X

https://doi.org/10.1016/j.finel.2013.11.006

Topology synthesis of Multi-Material compliant mechanisms with a Sequential Element Rejection and Admission method

Cristina Alonso Gordoa*
Department of Mechanical Engineering
University of The Basque Country
Alda, Urquijo s/n, 48013 Bilbao, Spain
Telephone: 0034946014092
Fax: 0034946014215
E-mail: calonso015@ikasle.ehu.es

Rubén Ansola Loyola
Department of Mechanical Engineering
University of The Basque Country
Alda, Urquijo s/n, 48013 Bilbao, Spain
Telephone: 0034946014092
Fax: 0034946014215
E-mail: ruben.ansola@ehu.es

Osvaldo M. Querin
School of Mechanical Engineering
University of Leeds
Leeds LS2 9JT, United Kingdom
Telephone: +441133432218
E-mail: O.M.Querin@leeds.ac.uk

*Corresponding author

Abstract

The design of multi-material compliant mechanisms by means of a multi Sequential Element Rejection and Admission (SERA) method is presented in this work. The SERA procedure was successfully applied to the design of single-material compliant mechanisms. The main feature is that the method allows material to flow between different material models. Separate criteria for the rejection and admission of elements allow material to redistribute between the pre-defined material models and efficiently achieve the optimum design. These features differentiate it to other bi-directional discrete methods, making the SERA method very suitable for the design of multi-material compliant mechanisms. Numerous examples are presented to show the validity of the multi SERA procedure to design multi-material compliant mechanisms.

Keywords

Topology optimization, compliant mechanisms, multiple materials, SERA method, output displacement

1 Introduction

Compliant mechanisms can be defined as monolitic structures that rely on its own elastic deformation to achieve force and motion transmission [1]. They have undergone considerable development since the introduction of both advanced materials and the field of MicroElectroMechanical Systems (MEMS). These submillimeter mechanical systems are the most promising application area of compliant mechanisms. They are coupled with electronic circuits and manufactured using etching techniques and surface micromachining processes from the semiconductor industry [2]. The use of hinges, bearings and assembly processes are prohibitive due to their small size, and must be built and designed as compliant mechanisms etched out of a single piece.

The most widely studied compliant mechanisms are single-material devices. Originally accomplished by trial and error methods, researchers took an interest in the systematic design of this type of compliant mechanisms by means of topology optimization techniques [3-5]. The main advantage of these techniques was that the optimum design was automatically suggested for a target volume fraction for a prescribed design domain, boundary conditions and functional specifications. There was no need to pre-determine the number of links or the location of the flexural joints in the device [6].

The optimization methods used for this purpose were diverse. Among others, the homogenization method [3, 7], the SIMP method [5], the Genetic Algorithms [8], the Level Set methods [9] and, more recently, the SERA method [10].

During the last decade, the design of devices with multiple materials gained popularity with the recent development of manufacturing methods. It is the case of the coextrusion of plastics, the shape deposition manufacturing [11], or the layered manufacturing with embedded components [12].

As a result, some of the methods applied to single-material compliant mechanisms were also applied to the design of multi-material compliant mechanisms. Sigmund [13]

performed topological synthesis of electrothermal actuators with nonlinear deformation and multiple materials and output ports. In this work, Sigmund studied the effect on the mechanisms performance of using two materials for thermal and electrothermal actuators. The conclusion was that the use of two materials was beneficial only in some cases and that those gains were, in many cases, insignificant. Yin and Ananthasuresh [14] proposed a peak function material interpolation scheme to incorporate multiple materials to the design of compliant mechanisms without increasing the number of design variables. In the two aforementioned works, the optimization methods used were gradient based with algorithms comprising the optimality criterion [14] or the method of moving asymtotes [13].

More recently developed methods were also applied to the design of multi-material compliant mechanisms. Wang and Chen [15] extended the Level Set approach to the design of monolithic compliant mechanisms made of multiple materials. The mechanical advantage of the mechanisms was used as objective function. Saxena [16] used Genetic Algorithms to compute the synthesis of compliant mechanisms with multiple materials and output displacements. Geometrically nonlinear analysis was used and the implementation was accomplished usign frame finite elements.

This research focuses on the design process for multi-material mechanisms and it can be used in multiple applications. It is the case, among others, of piezoelectric devices [24], bimorph actuators [13], grippers and clamping devices [15] or biologically inspired mechanisms in which multiple materials such as bones, muscles or skin are connected together to perform the desired function effectively [25]. It is specially interesting when: (a) One of the materials is more expensive; (b) the designer is interested in having a stiffer internal mechanism structure with flexible material surrounding it; (c) the designer is interested in mechanisms with porous materials; (d) there is a need to isolate a region and the inclusion of an electrically non-conductive phase in the mechanism design may make it possible; (e) a mechanism already exists and its output

displacement needs to be increased without changing its topology apart from reducing the size of the existing members and adding material around it.

The aim of this paper is to present a generalized formulation for the design of multi-material compliant mechanisms with the use of a Sequential Element Rejection and Admission (SERA) method [17,18]. This method was succesfully applied to the design of single-material compliant mechanisms [10]. The procedure considers two separate criteria for the rejection and admission of elements and material was redistributed between two material models: 'real' material and 'virtual' material with negligible stiffness. This feature of the SERA method makes it ideally suited for the design of multi-material compliant mechanisms. The formulation presented here is an extension from the one used for single-material compliant mechanisms [10] where the objective was to maximize the mutual potential energy of the mechanism under a constraint in the target volume fraction. Benchmark examples are used to demonstrate the validity of the proposed method to design multi-material compliant mechanisms.

2 Problem formulation of a multi-material compliant mechanism

A multi-material compliant mechanism is required to meet the flexibility and stiffness requirements in order to withstand the applied loads and produce the predefined displacement transmission. Fig. 1 shows such a multi-material compliant mechanism domain Ω. It is subjected to a forces F_{in} at the input port P_{in} and is supposed to produce an output displacements Δ_{out} at the output port P_{out}.

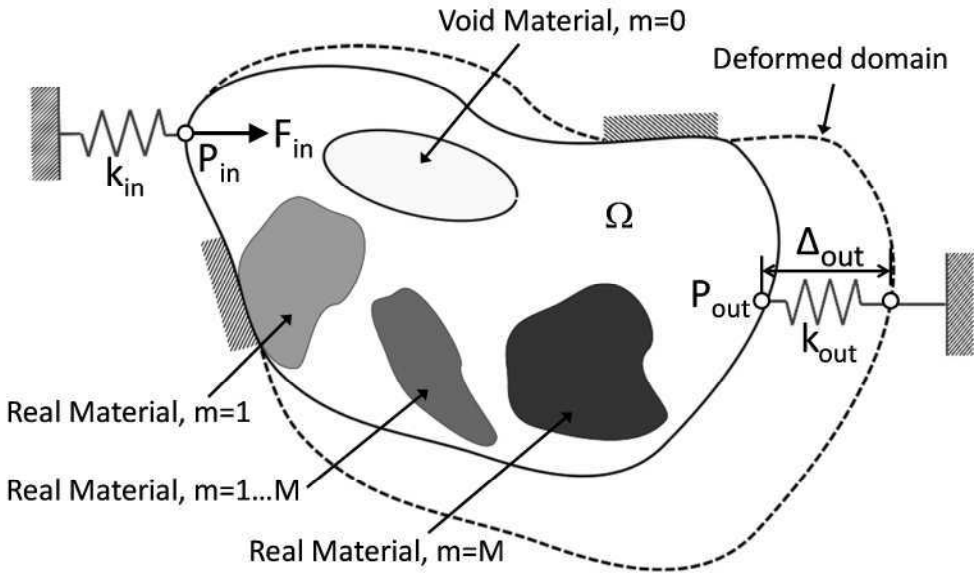

Fig. 1 Problem definition of a multi-material compliant mechanism

The goal of topology optimization for multi-material compliant mechanisms is to obtain the optimum design that converts the input work into an output displacement in a predefined direction. The mathematical formulation of this work is expressed as the maximization of the Mutual Potential Energy (MPE) (1) subjected to M constraints on the target volume fraction of the M materials, V^*_m (2). The summation of target volume fractions must be the unit (3) as each element can only be in one material model.

$$\max MPE \tag{1}$$

$$subjected\ to\colon\ for\ m = 0, \dots, M$$

$$\sum_{e=1}^{N} \rho_m^e \cdot \frac{V_m^e}{V_{Tot}} \leq V_m^* , \qquad \rho_m^e = \{\rho_{min}, 1\}, \qquad e = 1, \dots, N \tag{2}$$

$$\sum_{m=0}^{M} V_m^* = 1 , \qquad m = 0, \dots, M \tag{3}$$

where: $\rho^e{}_m$ is the density of the e^{th} finite element and material m, V_m^e is the volume of the e^{th} element and material m, V_{Tot} is the total volume for the domain, M is the number

of materials, N is the number of finite elements and ρ_{min} is the minimum density considered, a typical value of which is 10^{-4}. Void material is represented with m=0.

The MPE (4) [19] was defined as the deformation at a prescribed output port in a specified direction. To obtain the MPE, two load cases are calculated: 1) The Input Force Case, where the input force F_{in} is applied to the input port P_{in}, named with the subscript 1 in (4, 5) and Fig. 2a ; 2) the Pseudo-Force Case, where a unit force is applied at the output port P_{out} in the direction of the desired displacement, named with the subscript 2 in (4, 6) and Fig. 2b.

$$MPE = \boldsymbol{U}_2^T \cdot \boldsymbol{K} \cdot \boldsymbol{U}_1 \tag{4}$$

$$\boldsymbol{K} \cdot \boldsymbol{U}_1 = \boldsymbol{F}_1 \tag{5}$$

$$\boldsymbol{K} \cdot \boldsymbol{U}_2 = \boldsymbol{F}_2 \tag{6}$$

where: $\boldsymbol{K}$ is the global stiffness matrix of the structure; $\boldsymbol{F}_1$ is the nodal force vector which contains the input force F_{in}; $\boldsymbol{F}_2$ is the nodal force vector which contains the unit output force F_{out}; and $\boldsymbol{U}_1$, $\boldsymbol{U}_2$ are the displacement fields due to each load case.

The global stiffness matrix $\boldsymbol{K}$ is expressed by the density of the e^{th} finite element and the elemental stiffness matrix (7).

$$\boldsymbol{K} = \sum_{\mathrm{e}}^{\mathrm{N}} \rho_{\mathrm{m}}^{\mathrm{e}} \cdot \mathrm{K}_{\mathrm{m}}^{\mathrm{e}}(\mathrm{E}_{\mathrm{m}}, \upsilon_{\mathrm{m}}) , \qquad m = 0, \dots, M, \mathrm{e} = 1, \dots, \mathrm{N} \tag{7}$$

where: K^e_m is the elemental stiffness matrix of the e^{th} element, which depends on the Young modulus E_m and Poisson ratio υ_m of the m isotropic material.

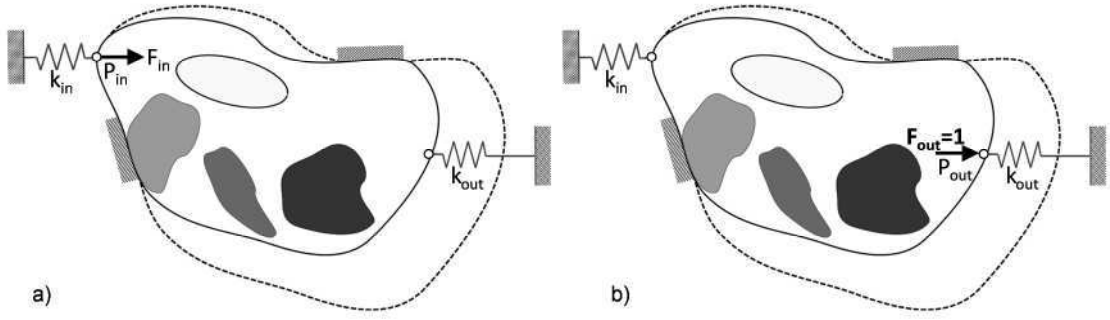

Fig. 2 Representation of the load cases: a) Case1: Input Force; b) Case 2: Pseudo-Force

The definition of the stiffness at the input and output ports is done in this work with the use of the spring model of Fig. 1. The artificial input spring k_{in} together with an input force F_{in} simulates the input work of the actuator. The resistance to the output displacement is modelled with a spring of stiffness k_{out}. This allows the displacement amplification to be controlled by specifying different values of the input and output springs.

As part of the optimization process, a sensitivity analysis is carried out to provide information on how sensitive the objective function is to small changes in the design variables. The derivative of the MPE with respect to the element density is given in (8).

$$\frac{\partial MPE}{\partial \rho_e} = \frac{\partial}{\partial \rho_e}(\boldsymbol{U}_2^T \cdot \boldsymbol{K} \cdot \boldsymbol{U}_1) = (\frac{\partial \boldsymbol{U}_2^T}{\partial \rho_e} \cdot \boldsymbol{K} \cdot \boldsymbol{U}_1 + \boldsymbol{U}_2^T \cdot \frac{\partial \boldsymbol{K}}{\partial \rho_e} \cdot \boldsymbol{U}_1 + \boldsymbol{U}_2^T \cdot \boldsymbol{K} \cdot \frac{\partial \boldsymbol{U}_1}{\partial \rho_e}) \tag{8}$$

Since the stiffness matrix is symmetric, the first derivative is then given in (9).

$$\frac{\partial \boldsymbol{U}_2^T}{\partial \rho_e} \cdot \boldsymbol{K} \cdot \boldsymbol{U}_1 = (\boldsymbol{K} \cdot \boldsymbol{U}_1)^T \cdot \frac{\partial \boldsymbol{U}_2}{\partial \rho_e} = \boldsymbol{U}_1^T \cdot \boldsymbol{K}^T \cdot \frac{\partial \boldsymbol{U}_2}{\partial \rho_e} = \boldsymbol{U}_1^T \cdot \boldsymbol{K} \cdot \frac{\partial \boldsymbol{U}_2}{\partial \rho_e} \tag{9}$$

Giving the derivative of the MPE to be (10).

$$\frac{\partial MPE}{\partial \rho_e} = (\boldsymbol{U}_1^T \cdot \boldsymbol{K} \cdot \frac{\partial \boldsymbol{U}_2}{\partial \rho_e} + \boldsymbol{U}_2^T \cdot \frac{\partial \boldsymbol{K}}{\partial \rho_e} \cdot \boldsymbol{U}_1 + \boldsymbol{U}_2^T \cdot \boldsymbol{K} \cdot \frac{\partial \boldsymbol{U}_1}{\partial \rho_e}) \tag{10}$$

The two equilibrium equations (5) and (6) are differentiated with respect to the density and are given in (11) and (12). The input load is independent from the design variables and its derivative is zero.

$$\frac{\partial \boldsymbol{K}}{\partial \rho_e} \cdot \boldsymbol{U}_1 + \boldsymbol{K} \cdot \frac{\partial \boldsymbol{U}_1}{\partial \rho_e} = 0 \rightarrow \frac{\partial \boldsymbol{K}}{\partial \rho_e} \cdot \boldsymbol{U}_1 = -\boldsymbol{K} \cdot \frac{\partial \boldsymbol{U}_1}{\partial \rho_e} \tag{11}$$

$$\frac{\partial \boldsymbol{K}}{\partial \rho_e} \cdot \boldsymbol{U}_2 + \boldsymbol{K} \cdot \frac{\partial \boldsymbol{U}_2}{\partial \rho_e} = 0 \rightarrow \frac{\partial \boldsymbol{K}}{\partial \rho_e} \cdot \boldsymbol{U}_2 = -\boldsymbol{K} \cdot \frac{\partial \boldsymbol{U}_2}{\partial \rho_e} \tag{12}$$

The equivalences obtained in (11) and (12) are introduced to (10), giving the derivative of the MPE to be (13).

$$\frac{\partial MPE}{\partial \rho_e} = \left(-\boldsymbol{U}_1^T \cdot \frac{\partial \boldsymbol{K}}{\partial \rho_e} \cdot \boldsymbol{U}_2 - \boldsymbol{U}_2^T \cdot \boldsymbol{K} \cdot \frac{\partial \boldsymbol{U}_1}{\partial \rho_e} + \boldsymbol{U}_2^T \cdot \boldsymbol{K} \cdot \frac{\partial \boldsymbol{U}_1}{\partial \rho_e}\right) = -\boldsymbol{U}_1^T \cdot \frac{\partial \boldsymbol{K}}{\partial \rho_e} \cdot \boldsymbol{U}_2 \quad (13)$$

As each density variable corresponds to a unique mesh element, only the displacements and stiffness of that element needs to be considered in the calculation. The sensitivity number for an element *e*, α_e can be calculated using (14).

$$\alpha_e = -\boldsymbol{U}_{1e}^T \cdot \frac{\partial \boldsymbol{K}_{\mathrm{m}}^{\mathrm{e}}}{\partial \rho_{\mathrm{m}}^{\mathrm{e}}} \cdot \boldsymbol{U}_{2e} \quad (14)$$

where: $\boldsymbol{U}_{1e}$ is the displacement vector of element *e* due to load case 1; $\boldsymbol{U}_{2e}$ is the displacement vector of element *e* due to load case 2; and $\frac{\partial \boldsymbol{K}_{\mathrm{m}}^{\mathrm{e}}}{\partial \rho_{\mathrm{m}}^{\mathrm{e}}}$ is the derivative of the elemental stiffness matrix with respect to the density.

The derivative of the stiffness matrix with respect to the density can only be approximated to the variation of the elemental stiffness (15). This is because the design variables are discrete (density can only be zero or one) and as a consequence, the elemental stiffness can only be the value of the stiffness of the *m* real material, $\boldsymbol{K}_{\mathrm{m}}^{\mathrm{e}}$ or a negligible value equivalent to zero.

$$\frac{\partial \boldsymbol{K}_{\mathrm{m}}^{\mathrm{e}}}{\partial \rho_{\mathrm{m}}^{\mathrm{e}}} \approx \Delta \boldsymbol{K}_{\mathrm{m}}^{\mathrm{e}} \quad (15)$$

When the approximation to the variation of the elemental stiffness in (15) is substituted to the expression of the elemental sensitivity number (14) and the relative volume of the FE is factored, equation (16) is obtained. This sensitivity number in each element (16) determines which elements are removed or added so that the objective function is maximized.

$$\alpha_e = (-\boldsymbol{U}_{1e}^T \cdot \Delta \boldsymbol{K}_{\mathrm{m}}^{\mathrm{e}} \cdot \boldsymbol{U}_{2e}) \cdot \frac{\mathrm{V}_{\mathrm{m}}^{\mathrm{e}}}{\mathrm{V}_{\mathrm{Tot}}} \quad (16)$$

where: $\boldsymbol{U}_{1e}$ is the displacement vector of element *e* due to the applied load $\mathbf{F}_1$; $\boldsymbol{U}_{2e}$ is the displacement vector of element *e* due to the output load vector $\mathbf{F}_2$; and $\Delta \boldsymbol{K}^e_m$ is the variation of the elemental stiffness matrix.

3 The SERA method for multi-material compliant mechanisms design

The SERA method was originally defined for single-material structures. It considered two separate material models: 1) 'Real' material and 2) a 'Virtual' material with negligible stiffness [17, 18]. Two separate criteria allowed material to be introduced and removed from the design domain by changing its status from 'virtual' to 'real' and vice versa [10].

In the SERA method for multi-material compliant mechanisms, the definition of separate criteria for each material model is maintained. The method is extended for multiple materials so that elements can flow between consecutive levels of material models. Elements in material model *m* "move forward" to material model *(m+1)* or "move backwards" to material model *(m-1)*. The final topology is made of all the different 'real' materials m= [1, M] present at the end of the optimization (Fig. 3).

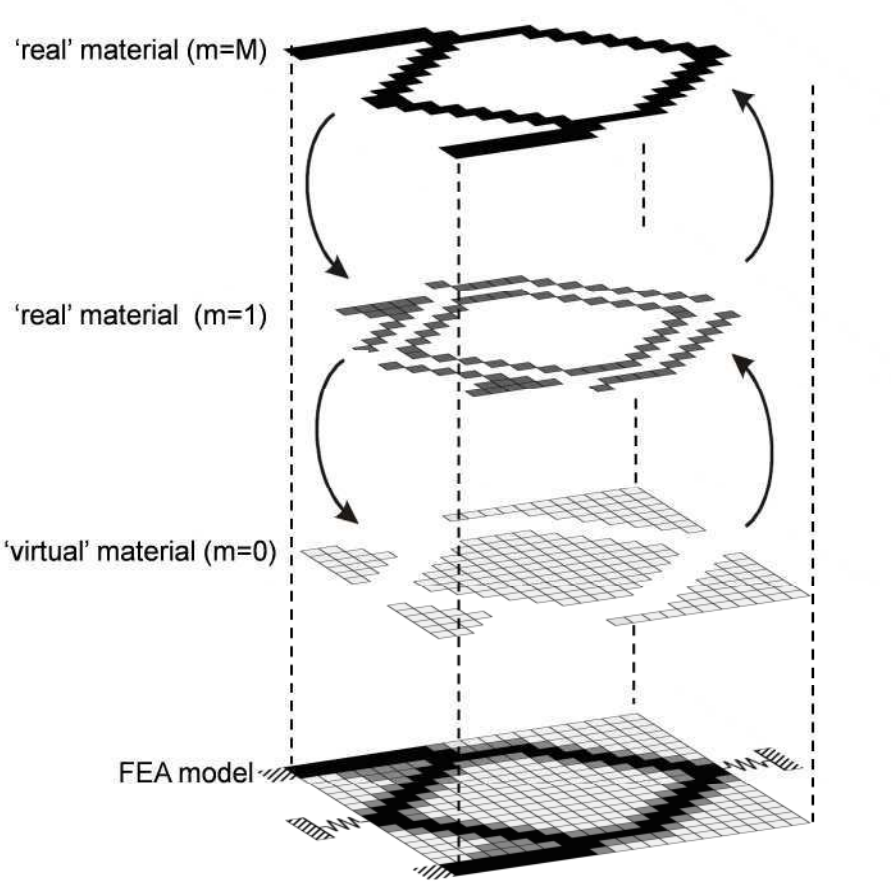

Fig. 3 The SERA material models for multi-material compliant mechanisms

The twelve steps that drive the SERA method for multi-material compliant mechanisms are given below, and can be seen in the flow chart of Fig 4.

1. Define the design problem. The maximum design domain must be defined and meshed with finite elements. All boundary constraints, loads and the target volume fraction for each material model V^*_m must also be specified.
2. Define properties for each material model and assign material properties to the initial design domain, section 3.1.
3. Calculate the amounts of volume to redistribute in the i^{th} iteration which consists of the volume to be "moved forward" $\Delta V_{Fw,m}(i)$ and "moved backwards" $\Delta V_{Bw,m}(i)$ in each material model m, section 3.2.
4. Carry out a Finite Element Analysis of the two load cases to produce the displacement vectors $\boldsymbol{U}_1$ and $\boldsymbol{U}_2$. The elemental and global stiffness matrixes, $\boldsymbol{K}^e_m$ and $\boldsymbol{K}$, are also calculated as part of the FEA.
5. Calculate the elemental sensitivity numbers α_e (16).
6. Apply the mesh independent filtering to the sensitivity numbers, section 3.3.
7. Separate the sensitivity numbers in those for each material model, $\boldsymbol{\alpha}_m$.
8. Define the threshold values for each material model, $\alpha_{Fw,m}{}^{th}$ and $\alpha_{Bw,m}{}^{th}$, section 3.4.
9. Redistribution of elements between material models, section 3.4.
10. Calculate the volume of each 'real' material model and the total volume of 'real' material in the domain.
11. Calculate the convergence criterion ε_i, section 3.5.
12. Repeat steps (3) through (11) until the target volume fractions are reached and the optimization converges. The final topology is represented by the 'real' material in the design domain.

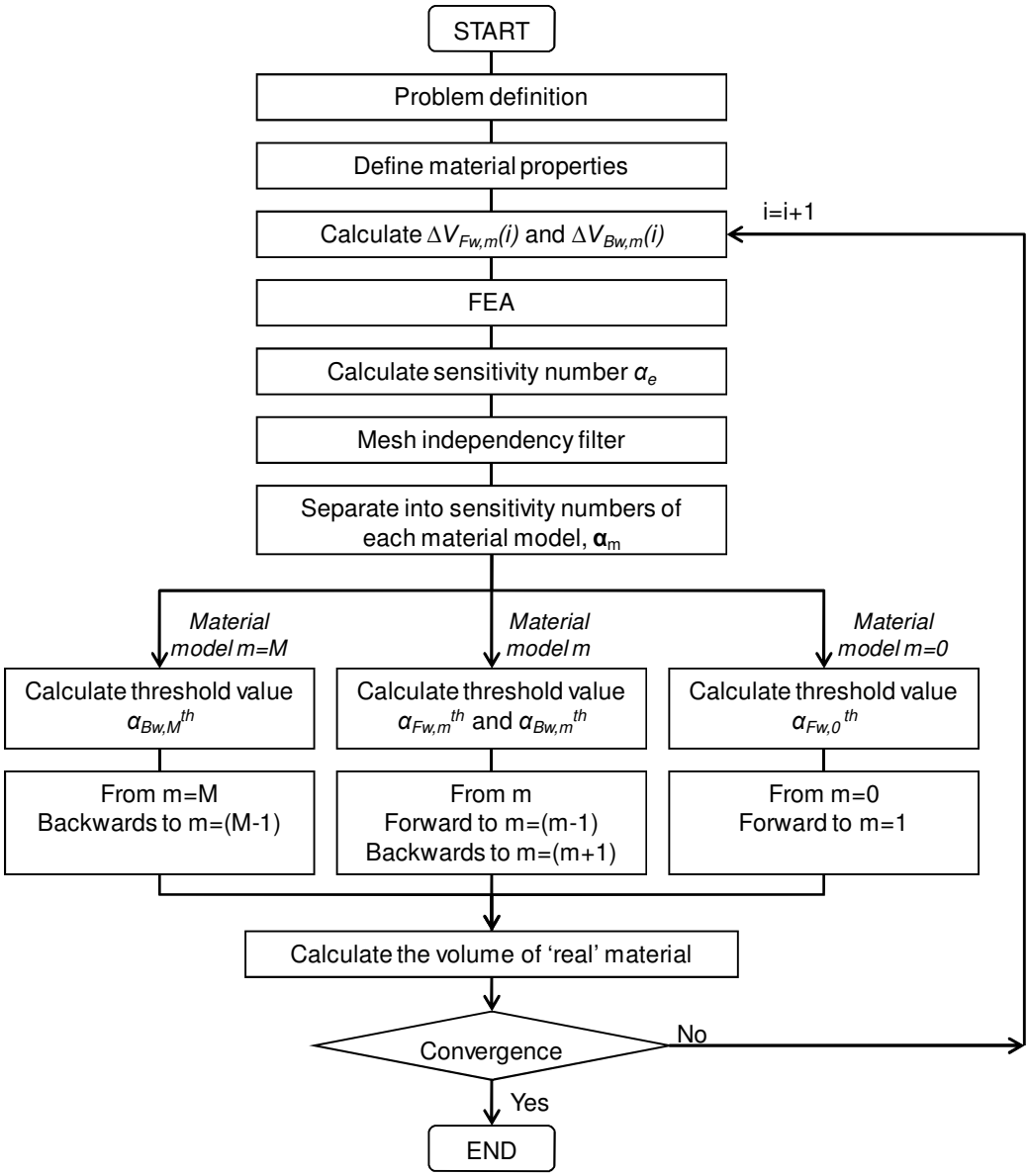

Fig. 4 Flow chart of the SERA method for multi-material compliant mechanisms

3.1. Definition of material properties

The SERA method can start from a full design domain (all elements are 'real' material), from a void design domain (all elements are 'virtual' material), and also with any amount of material present in the domain. In a previous work by the authors [20], it was stated that a void initial design domain was the most efficient starting point to design compliant mechanisms as fewer iterations were needed to achieve the optimum. This

is the strategy considered in this work and, therefore, all elements in the design domain are assigned 'virtual' material properties as the initial design domain.

The rest of material models (m=1...M) are initialized so that m=1 is the weakest 'real' material available and m=M the one with higher material properties. That is, elements "move forward" from 'void' material towards material M.

3.2. Calculating the volumes $\Delta V_{Fw,m}(i)$ and $\Delta V_{Bw,m}(i)$

Material is moved between material models in a two stage process (Fig. 5):

1. Different amounts of material are moved forward and backwards in each iteration until the target volume fraction for each material model V_m^* is reached.
2. Once the target volume fractions of each material model are reached, material re-distribution takes place by moving the same amount of material between material models until the problem converges.

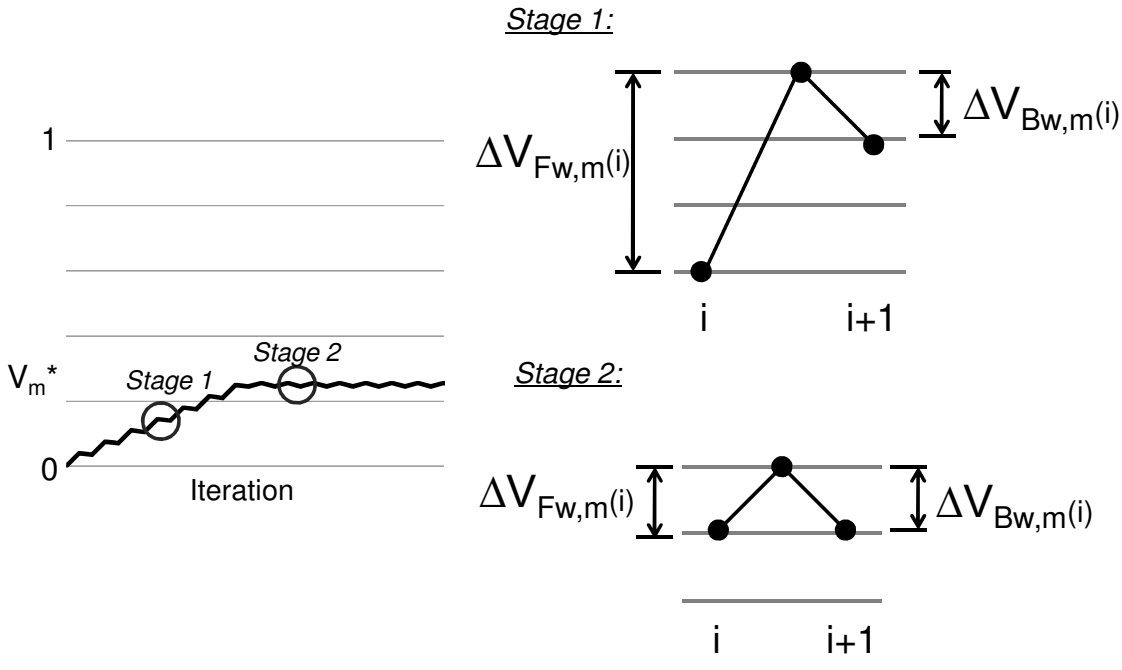

Fig. 5 Scheme of the volume to move forward and backwards for material m

The volume of material to be moved forward and backwards are given in equations (17) and (18) when an equal target volume fraction V_m^* is to be achieved in all 'real'

material models. This can be adjusted for any other relationship between target volume fractions.

$$\Delta V_{Bw,m}(i) = PR \cdot N, \qquad for\ m = 1 \dots M \tag{17}$$

$$\Delta V_{Fw,m}(i) = PR \cdot N \cdot (M + 1 - m), \qquad for\ m = 0 \dots (M - 1) \tag{18}$$

where: *PR* is the progression rate, with typical values ranging between 0.005-0.05; *N* is the number of finite elements.

The stage of material re-distribution consists of redistributing material without increasing the total in each material model (19) (20).

$$\Delta V_{Bw,m}(i) = RR \cdot N, \qquad for\ m = 1 \dots M \tag{19}$$

$$\Delta V_{Fw,m}(i) = RR \cdot N \cdot, \qquad for\ m = 0 \dots (M - 1) \tag{20}$$

where: RR is the material Re-distribution Rate, with typical values ranging between 0.001 and 0.005.

3.3. Mesh independent filtering

The mesh independent filter is based on the one by Sigmund and Petersson [21] and modifies the sensitivity number of each element based on a weighted average of the element sensitivities (21) in a fixed neighbourhood defined by a minimum radius r_{min} (22).

$$\alpha_e^{'} = \frac{\sum_{k=1}^{n} \rho_k \cdot \omega_k \cdot \alpha_k}{\sum_{k=1}^{n} \omega_k} \tag{21}$$

$$\omega_k = r_{min} - dist(e,k), \qquad \{k\ \in n\ /\ dist(e,k) \leq r_{min}\}, \qquad e = 1, \dots, n \tag{22}$$

where: α'_e is the e^{th} element filtered sensitivity number. *n* is the number of elements which are inside of the filter radius. ρ_k is the density of element *k*. ω_k is the weighting factor for element *k*, its value decreases linearly the further element *k* is away from element *e* and for all elements outside the filter radius its value is equal to zero. α_k is

the k^{th} element sensitivity value. r_{min} is the filter radius specified by the user. *dist(e,k)* is the distance between the centres of elements *e* and *k*.

3.4. Redistribution of material

The sensitivity numbers of each e^{th} finite element α_e (16) are listed separately in (M+1) lists, one for each material model m=0...M (Fig 6).

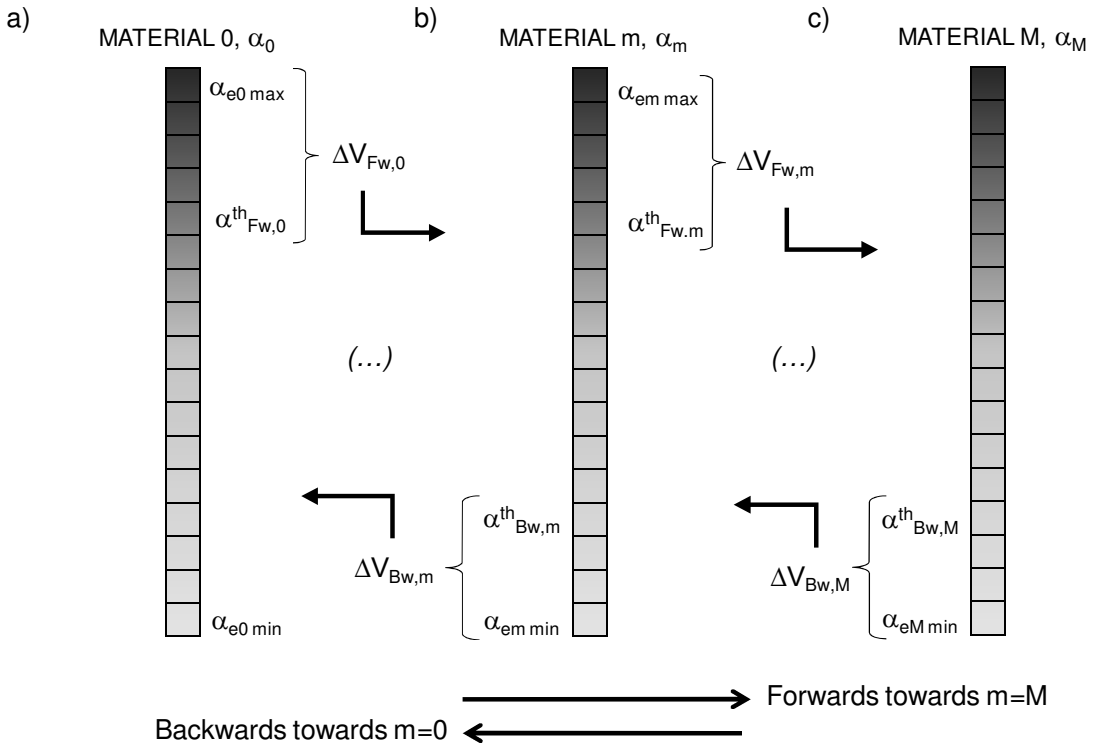

Fig. 6 Scheme of the lists of material models and the volumes to move forwards and backwards

The threshold values $\alpha_{Fw,m}{}^{th}$ and $\alpha_{Bw,m}{}^{th}$ are the sensitivity values that allows the transmission of $\Delta V_{Fw,m}(i)$ from material *m* to material *(m+1)*, and $\Delta V_{Bw,m}(i)$ from material *m* to material *(m-1)* (Fig. 6).

The objective is to maximize the MPE and, therefore, in general for material *m*: elements with the higher values of sensitivity number are the ones to be moved forward to the next material model *(m+1)*. Elements with lower values of sensitivity number are the ones to be moved backwards to the previous material model *(m-1)* (Fig. 6b).

Special cases of this rule are material models m=0 and m=M. For m=0, elements can only be forwarded to material model m=1 (Fig. 6a). For m=M, material can only be moved backwards to the previous material model (Fig. 6c).

3.5. Convergence criterion

The convergence criterion is defined as the change in the objective function in the last 10 iterations (23), which is considered an adequate number of iterations for the convergence study. It implies that the process will have a minimum of 10 iterations as the convergence criterion is not applied until the iteration number has reached 10.

$$\varepsilon_i = \frac{\left|\sum_{i-9}^{i-5} MPE_i - \sum_{i-4}^{i} MPE_i\right|}{\sum_{i-4}^{i} MPE_i} \tag{23}$$

when: ε_i is the convergence criterion, with typical values ranging between 0.001-0.01.

4 Examples

Examples of multi-material compliant mechanisms are presented in this section to demonstrate the validity of the proposed method: 1) Bi-material inverter mechanisms, 2) Bi-material crunching mechanisms, and 3) Tri-material gripper mechanisms.

For the inverter mechanism, different target volume fractions for the two material models are considered. In the case of the crunching mechanisms, different target volume fractions and material properties are used for compliant mechanisms with different stiffness ratios. Finally, two different designs of tri-material gripper mechanisms are presented. The evolution charts of these two optimization processes are also given in this section.

4.1. Bi-material inverter mechanism with different target volume fractions

The design domain for an inverter mechanism is shown in Fig. 7. It is a square of size 120x120mm subdivided using square four node 2x2mm finite elements.

Two real materials are considered: Material m=1 with E_1=0.1, v_1=0.3, and Material m=2 with E_2=1, v_2=0.3. That is, material 2, represented in black in the figure, is ten times stiffer than material 1, represented in orange in the figure. The density of the virtual material m=0 is $\rho_{min}=10^{-4}$, which is equivalent to 0.01% of the stiffness of a real material.

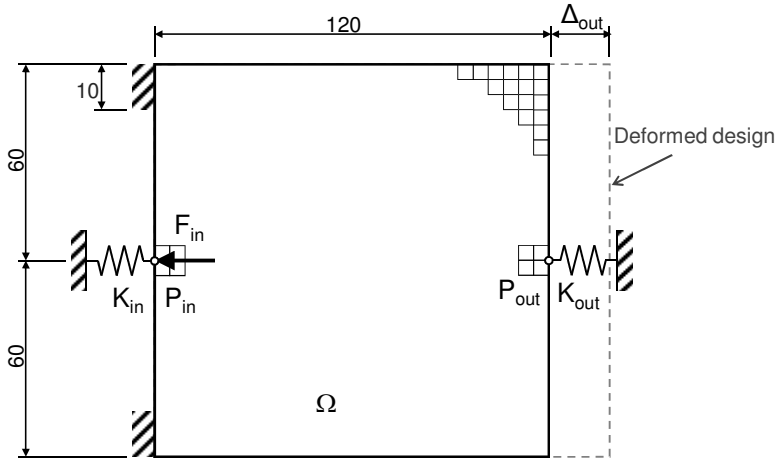

Fig. 7 Inverter mechanism (all dimensions are in mm)

The two target volumes fractions considered are: a) V_1*=0.2, V_2*=0.2, b) V_1*=0.1, V_2*=0.3 of the initial design domain. In both cases, the same input force F_{in}=1N is applied and a stiffness ratio between the input and output ports of k_{out}/k_{in}=1 is defined. The filter radius used in all cases is r_{min}=4mm. The final topologies obtained for the two cases are shown in Fig. 8.

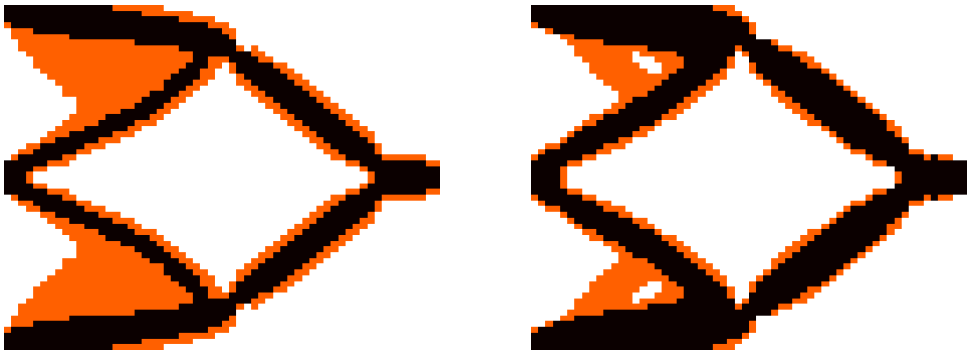

(a) (b)

Fig. 8 Inverter mechanisms with: a) V_1=0.2, V_2*=0.2, b) V_1*=0.1, V_2*=0.3*

As it can be observed in Fig. 8, material is efficiently distributed in the design domain in order to transmit the motion from the input to the output port. Regarding the distribution of each material model, the stiffest one defines a topology capable of providing the transmission of movement and the weakest material is located where it provides stability to the mechanisms without reducing its capacity of movement.

4.2. Bi-material crunching mechanism with different stiffness ratios

The design domain for the crunching mechanism is shown in Fig. 9. It is a square of size 120x120mm subdivided using square four node 2x2mm finite elements.

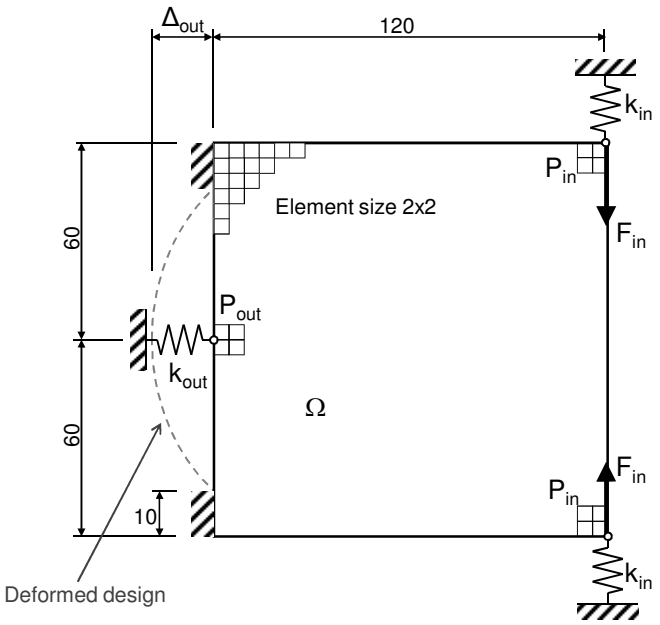

Fig. 9 Crunching mechanism (all dimensions are in mm)

Three different input-output situations are considered in this section: 1) $k_{out}/k_{in}=0.01$, 2) $k_{out}/k_{in}=1$, 3) $k_{out}/k_{in}=100$. The topologies obtained for single-material mechanisms (Alonso *et al.* 2012) were significantly different so it could be thought that the inclusion of a second material could beneficiate the mechanisms performance in, at least, some of the cases. Two different volume distribution for the bi-material mechanisms are also considered: 1) $V_1^*=0.2$, $V_2^*=0.2$, and 2) $V_1^*=0.3$, $V_2^*=0.1$ (cases (b),(c), and (d)). All the rest of parameters remain unchanged ($F_{in}=1N$, $r_{min}=6mm$).

For each stiffness ratio, five cases of real material properties are studied: a) Single-material with E_1=1 and V_1*=0.4, V_2*=0, b) Bi-material with E_1=2·E_2 , c) Bi-material with E_1=10·E_2, d) Bi-Material with E_1=100·E_2, and e) Single-material with E_1=1 and V_1*=0.2, V_2*=0. For all cases, the Poisson's ratio is υ_1= υ_2=0.3 and the density of the virtual material m=0 is ρ_{min}=10^{-4}. Results are shown in Fig. 10, Fig. 11 and Fig. 12.

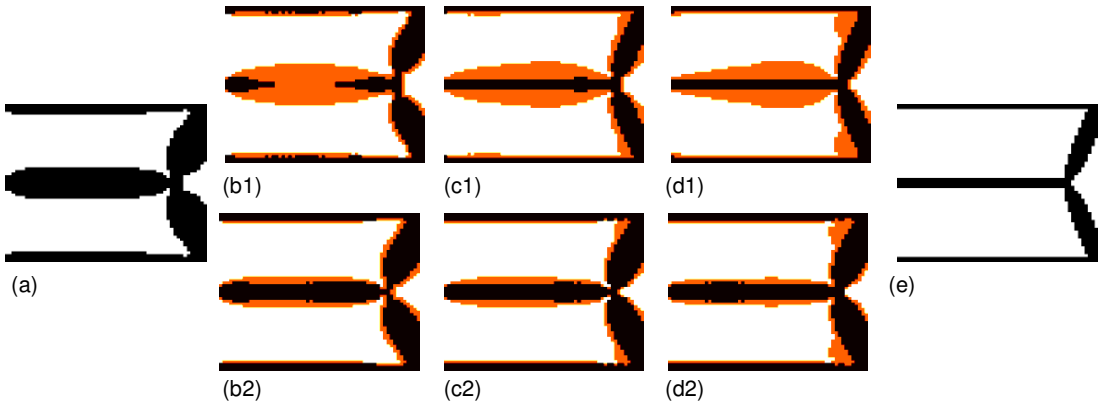

Fig. 10 Bi-Material crunching mechanism with k_{out}/k_{in}=0.01 and: a) E_1=1, V_1=0.4, b) E_1=2·E_2 with b1) V_1*=0.2, V_2*=0.2 and b2) V_1*=0.3, V_2*=0.1, c) E_1=10·E_2 with c1) V_1*=0.2, V_2*=0.2 and c2) V_1*=0.3, V_2*=0.1, d) E_1=100·E_2 with c1) V_1*=0.2, V_2*=0.2 and d2) V_1*=0.3, V_2*=0.1, and e) E_1=1, V_1*=0.2*

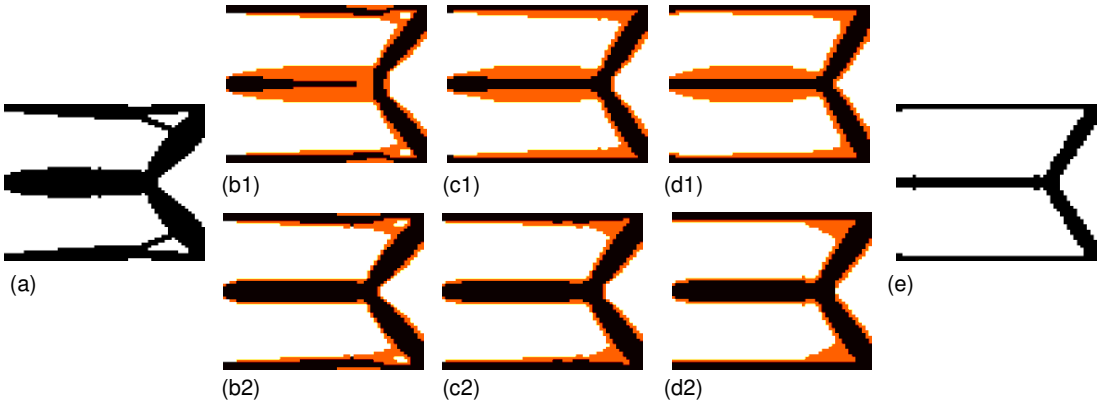

Fig. 11 Bi-Material crunching mechanism with k_{out}/k_{in}=1 and: a) E_1=1, V_1=0.4, b) E_1=2·E_2 with b1) V_1*=0.2, V_2*=0.2 and b2) V_1*=0.3, V_2*=0.1, c) E_1=10·E_2 with c1) V_1*=0.2, V_2*=0.2 and c2) V_1*=0.3, V_2*=0.1, d) E_1=100·E_2 with c1) V_1*=0.2, V_2*=0.2 and d2) V_1*=0.3, V_2*=0.1, and e) E_1=1, V_1*=0.2*

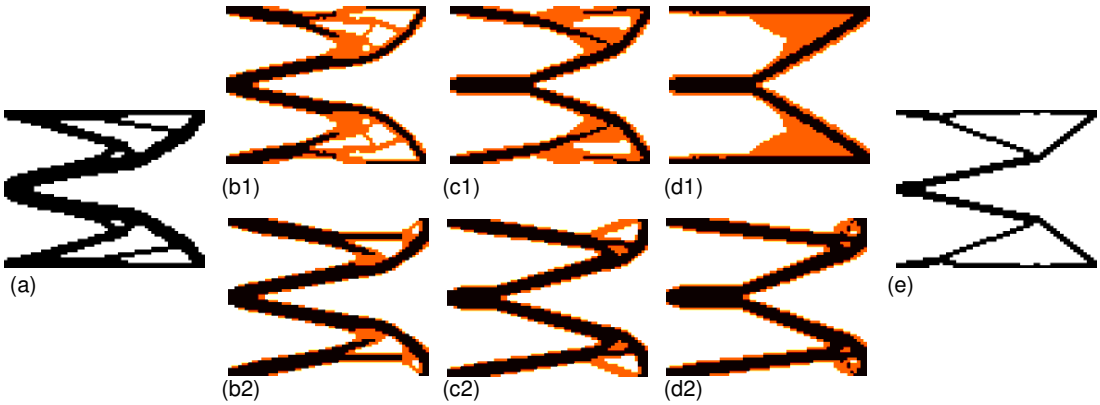

Fig. 12 Bi-material crunching mechanism with $k_{out}/k_{in}=100$ and: a) $E_1=1$, $V_1^*=0.4$, b) $E_1=2\cdot E_2$ with b1) $V_1^*=0.2$, $V_2^*=0.2$ and b2) $V_1^*=0.3$, $V_2^*=0.1$, c) $E_1=10\cdot E_2$ with c1) $V_1^*=0.2$, $V_2^*=0.2$ and c2) $V_1^*=0.3$, $V_2^*=0.1$, d) $E_1=100\cdot E_2$ with c1) $V_1^*=0.2$, $V_2^*=0.2$ and d2) $V_1^*=0.3$, $V_2^*=0.1$, and e) $E_1=1$, $V_1^*=0.2$

It can be observed from Fig. 10, Fig. 11 and Fig. 12, that the topology of bi-material crunching mechanism changes considerably if different material properties are defined for each material model (cases (b), (c), and (d)). In all cases, the SERA method proposed provides an efficient distribution of material in the design domain.

An analysis of the displacements in this and previous section reveal that all displacements are between 0.0012% and 0.9% of the dimensions of the mechanism. Due to such small displacements, the use of linear analysis with small displacements is appropriate for this work. The conclusions drawn from this study are based on the comparison of the performance of all examples under the same type of analysis and displacement range.

4.3. Tri-material gripper mechanisms

The design domain for two different gripper mechanisms are shown in Fig. 13. In both cases, it is a square of size 200x200mm subdivided using square four node 2x2mm finite elements. In case (a) a 50x50mm square in the right side is removed from the design domain to allow the mechanism to grip the workpiece, modelled by the output spring k_{out}. In case (b) the square is 150x50mm size.

Three real materials are considered: Material m=1 with E_1=0.01, v_1=0.3, Material m=2 with E_2=0.1, v_2=0.3, and Material m=3 with E_3=1, v_3=0.3. The density of the virtual material m=0 is $\rho_{min}=10^{-4}$.

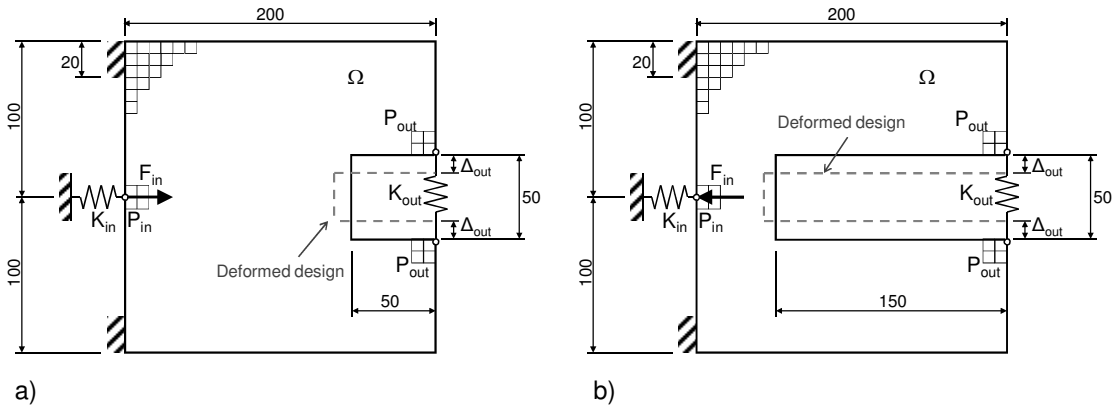

Fig. 13 Gripper mechanisms (all dimensions are in mm)

The target volume fractions considered for each material model are $V_1^*=V_2^*= V_3^*=0.15$ of the initial design. An input force F_{in}=1N is applied and a stiffness ratio of $k_{out}/k_{in}=1$ is defined. The filter radius used in all cases is r_{min}=6mm. The resulting topology and evolution chart of the gripper mechanism (a) case is shown in Fig. 14. The equivalent for the gripper mechanism (b) case is shown in Fig. 15. As it can be observed, in both cases, the three materials are efficiently distributed in the design domain.

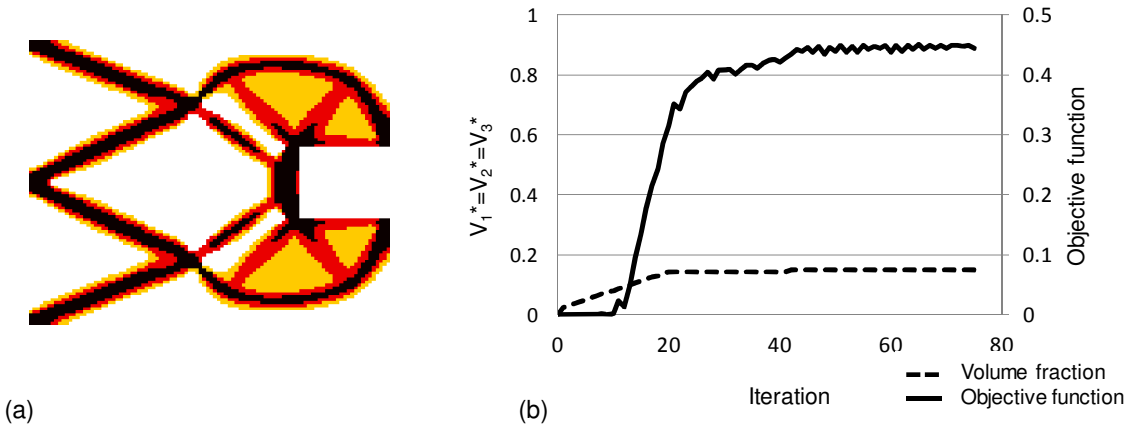

Fig. 14 Tri-material gripper mechanism (a) case: a) Final topology and b) evolution chart

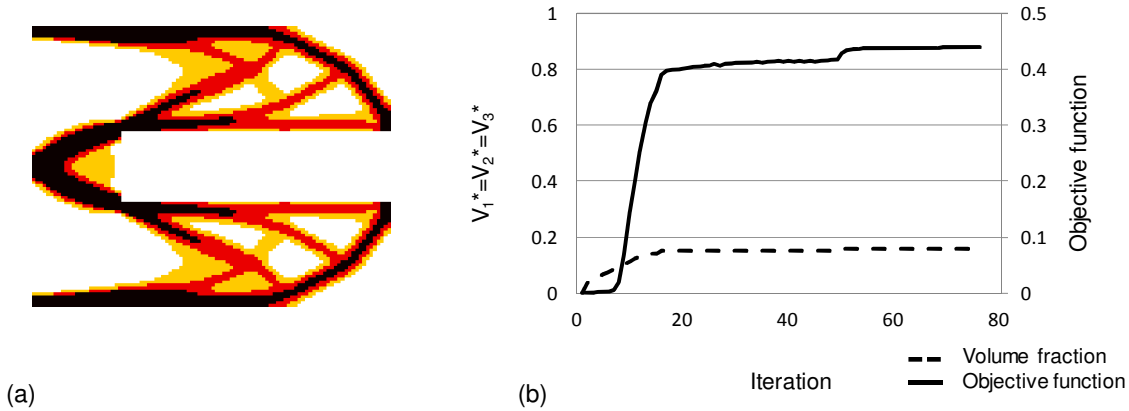

Fig. 15 Tri-material gripper mechanism (b) case: a) Final topology and b) evolution chart

5 Conclusions

A generalized formulation to design multi-material compliant mechanisms is presented in this work. A multi Sequential Element Rejection and Admission (SERA) method is used to achieve the optimum design. This procedure considers each material in the domain as separate material models. The rejection and admission of elements is done via separate criteria for each material model and elements flow between pre-defined material models. The examples presented in this work show the versatility and robustness of the method to achieve the optimum topology for compliant mechanisms with multiple materials.

The authors are aware of the need for a nonlinear analysis when large displacements are considered in compliant mechanisms [22,23]. However, for the purpose of studying the validity of the method, a linear analysis has proven to be a good approximation as all examples exhibit small displacements.

The SERA method has efficiently distributed material in all bi- and tri-material mechanisms presented in this work. It has therefore been demonstrated to be an efficient and robust method for the design of multiple materials compliant mechanisms.

Acknowledgements

This work was partially supported by the *Departamento de Educación* of the *Gobierno de Navarra* with the PhD scholarship of Cristina Alonso Gordoa. Its support is greatly appreciated.

This work was also partially supported by the Ministry of Education and Science in Spain through the project DPI2012-36600 and the *Unidades de Investigación y Formación* (UFI11/29). Their support is also greatly appreciated.

References

[1] L. Howell, Compliant mechanisms, New York: John Wiley & Sons, 2001.

[2] K. Petersen, Silicon as a mechanical material, Proc. IEEE 70(5) (1982) 420-457.

[3] G.K. Ananthasuresh, S. Kota, Y. Gianchandani, Systematic synthesis of micro compliant mechanisms: preliminary results, Proc. 3rd National Conf of Appl Mech and Robot, Ohio, 2(82) (1993).

[4] M. Frecker, G.K. Ananthasuresh, N. Nishiwaki, N. Kikuchi, S. Kota, Topological synthesis of compliant mechanisms using multi-criteria optimization, ASME J. Mech. Des. 119 (1997) 238–245.

[5] O. Sigmund, On the Design of Compliant Mechanisms Using Topology Optimization, Mech Struct Mach 25(4) (1997) 493-524.

[6] M. Bendsoe, O. Sigmund, Topology Optimization: Theory, Method and Application, Berlin, Springer, 2003.

[7] G.K. Ananthasuresh, S. Kota, Y. Gianchandani, A methodical approach to the design of compliant micromechanisms, Solid State Sensor and Actuator Workshop (1994) 189-192.

[8] R. Parsons, S. Canfield, Developing genetic programming techniques for the design of compliant mechanisms, Struct. Multidisc. Optim. 24 (2002) 78-86.

[9] M. Yulin, W. Xiaoming, A level set method for structural topology optimization and its applications, Advances in Engineering Software 35 (2004) 415-441.

[10] C. Alonso, O.M. Querin, R. Ansola, A Sequential Element Rejection and Admission (SERA) method for compliant mechanisms design, Struct. Multidisc. Optim. (2012) DOI: 10.1007/s00158-012-0862-9.

[11] S. Rajagopalan, R. Goldman, K.H. Shin, V. Kumar, M. Cutkosky, D. Dutta, Representation of heterogeneous objects during design, processing and freeform-fabrication, Mater. Des. 22 (2001) 185–197.

[12] S.A. Bailey, J.G. Cham, M.R. Cutkosky, R.J. Full, Biomimetic robotic mechanisms via shape deposition manufacturing. In: Hollerbach J, Koditschek D (eds) Robot Research: the ninth international symposium. Springer, Berlin Heidelberg New York, 2000.

[13] O. Sigmund, Design of multiphysics actuators using topology optimization|part II: Two-material structures, Comput. Methods Appl. Engrg. (2001) 190.

[14] L. Yin and G.K. Ananthasuresh, Topology optimization of compliant mechanisms with multiple materials using a peak function material interpolation scheme, Structural and Multidisciplinary Optimization, 23 (1) (2001) 49–62.

[15] M. Wang, S. Chen, X. Wang, Y. Mei, Design of multimaterial compliant mechanisms using level set methods, ASME Journal of Mechanical Design, 127 (2005) 941-956.

[16] A. Saxena, Topology design of large displacement compliant mechanisms with multiple materials and multiple output ports. Struct Multidisc Optim 30 (2005) 477-490.

[17] G.I.N. Rozvany, O. Querin, Theoretical foundations of Sequential Element Rejections and Admissions (SERA) methods and their computational implementations in topology optimisation, Symposium on Multidisciplinary Analysis and Optimization (2002) Issue 5521.

[18] G.I.N. Rozvany and O.M. Querin, Combining ESO with rigorous optimality criteria, International, Journal of Vehicle Design 28(4) (2002) 294-299.

[19] R. Shield, W. Prager, Optimal Structural Design for Given Deflection, J. Appl. Math. Phys. 21 (1970) 513-523.

[20] C. Alonso, R. Ansola, O.M. Querin, J. Canales, Design of compliant mechanisms with a Sequential Element Rejection and Admission method, Proceedings of the 10th World Congress on Computational Mechanics (WCCM2012) , ISBN: 978-85-86686-70-2, paper Nr. 19501, Sao Paulo, Brazil, 2012.

[21] O. Sigmund, J. Petersson, Numerical instabilities in topology optimization: A survey on procedures dealing with checkerboards, mesh-dependencies and local minima. Struct Optim 16 (1998) 68-75.

[22] T.E. Bruns, D.A. Tortorelli, Topology optimization of non-linear elastic structures and compliant mechanisms, Computer Methods in Applied Mechanics and Engineering 190 (2001) 3443-3459.

[23] C.B.W. Pedersen, T. Buhl, O. Sigmund, Topology synthesis of large-displacement compliant mechanisms. International Journal for Numerical Methods in Engineering 50-12 (2001) 2683-2706.

[24] Z. Luo, L. Tong, J.W.P. Luo, M. Wang, M., Design of piezoelectric actuators using a multiphase level set method of piecewise constants. Journal of Computational Physics 228 (2009) 2643–2659.

[25] H. Zhou, K.L. Ting, Geometric modelling and synthesis of spatial multimaterial compliant mechanisms and structures using three-dimensional multilayer wide curves, Journal of mechanical design 131 (2009) 011005-1.